The technique for extracting initial parameters of longitudinal phase space of freshly injected bunches in storage rings and its applications

Hongshuang Wang,[1] Yimei Zhou,[2] and Yongbin Leng[3]

[1]*Shanghai Institute of Applied Physics, Chinese Academy of Sciences, Shanghai,201800, China*
[2]*Shanghai Advanced Research Institute, Chinese Academy of Sciences, Shanghai, 201204, China*
[3]*National Synchrotron Radiation Laboratory, University of Science and Technology of China, Hefei, 230026, China*

This paper presents a technique for extracting the initial parameters of the longitudinal phase space of freshly injected bunches in an electron storage ring. This technique combines the development of a single-bunch injection phase space simulation software with the establishment of a bunch-by-bunch data acquisition and processing system, enabling high-precision acquisition of the initial parameters of injected bunches during the injection process into the electron storage ring (including initial phase, initial bunch length, initial energy offset, initial energy spread, and initial energy chirp). The experiment utilizes a high-speed oscilloscope to capture the beam injection signals, which are then processed by a data processing script to calculate and extract the phase and bunch length evolution information of the injected bunches. The data acquisition length covers several thousand turns per capture, with a phase measurement accuracy of 0.2 ps and a bunch length measurement accuracy of 1 ps. Additionally, a single-bunch simulation software based on the mbtrack2 and PyQt5 packages has been developed. This software can simulate the phase space evolution of bunches under different initial conditions after injection. By employing a genetic algorithm and integrating experimental data with simulation data, it can obtain the optimized initial parameters of the injected bunches.

Keywords: injection transient, phase measurement, bunch length measurement, genetic algorithm

I. INTRODUCTION

In advanced synchrotron light sources, the injection process in the electron storage ring is a critical factor influencing beam quality and stability. Optimizing the injection process can reduce beam loss, enhance injection efficiency, and minimize interference with experiments[1, 2, 4**?** –12]. Therefore, in-depth research and optimization of the electron storage ring injection process are of significant theoretical and practical importance.

In the observation and analysis of the injection process, transverse injection technology has become relatively mature. For instance, the team at the University of Guilan proposed a multi-turn transverse injection scheme for a 3.5 GeV synchrotron storage ring[13], using short-pulse nonlinear kickers to achieve efficient beam injection. The core of the research focuses on how to achieve on-axis injection in the synchrotron storage ring by designing injection systems (such as septa and pulsed sextupole magnets), thereby improving the stability of the storage ring and reducing interference with the stored beam. Through simulations and theoretical analysis, this method has demonstrated several advantages over traditional off-axis injection, including reducing beam emittance growth and improving injection efficiency.

PLS-II(Pohang Light Source-II) uses particle tracking software ELEGANT to simulate and analyze transient behaviors in the transverse and longitudinal phase spaces during beam injection[14]. By studying the distribution of injected beam in both transverse and longitudinal phase spaces, the characteristics of the beam's behavior post-injection and the impact of system errors on beam capture efficiency are analyzed. The injection beam conditions and system error range required for high injection efficiency are determined experimentally, and the debugging of the injection system in practical operation is guided.

Currently, the arrival time and bunch length of freshly injected bunches are typically measured directly using streak cameras[15]. Streak cameras can capture changes in the longitudinal size of the bunch over a snapshot time, but they cannot simultaneously provide high time resolution and large dynamic range. Moreover, existing diagnostic tools struggle to measure parameters such as central energy, energy spread, and energy chirp directly and accurately[16, 17]. These parameters are crucial for optimizing the injection process and enhancing light source performance, but there is still a lack of effective experimental methods for precise characterization and analysis[18].

In light of the current research landscape, this paper proposes a novel technique for extracting the initial longitudinal phase space parameters of freshly injected bunches in electron storage rings. This technique employs a high-speed oscilloscope to capture beam signals during the injection process and integrates advanced data processing algorithms, enabling the acquisition of bunch phase and bunch length evolution within a single injection cycle. By combining this approach with a newly developed single-bunch tracking simulation software based on the mbtrack2 and PyQt5 packages, the technique not only achieves precise measurements of the initial energy offset, initial energy spread, and initial energy chirp of the injected bunches but also predicts and simulates the behavior of particle beams in the storage ring. This advancement provides a powerful tool for optimizing the injection process.

II. LONGITUDINAL BEAM DYNAMICS IN STORAGE RINGS

In particle storage rings, charged particles move around a circular orbit in the form of bunches and fill different buck-

ets. The main coordinates used to describe the longitudinal motion of a bunch are position L (or phase φ) and momentum p. Assuming the equilibrium particle coordinates are L_0 and p_0, for non-equilibrium particles (coordinates L and p), the following relationship holds:

$$\frac{\Delta L}{L_0} = \left\langle \frac{\eta}{\rho} \right\rangle \frac{\Delta p}{p_0} = \alpha_c \frac{\Delta p}{p_0} \tag{1}$$

where α_c is the momentum compaction factor, ΔL is the position difference between the non-equilibrium particle and the equilibrium particle, Δp is the momentum difference, η is the dispersion function, and ρ is the curvature radius.

As particles move around the ring, they are accelerated by the electric field in the RF cavity, gaining energy, and then lose energy due to synchrotron radiation in the bending magnets. This establishes a dynamic balance, and the total energy change is given by the sum of these two terms:

$$\Delta E = qV(\psi) - U(E) \tag{2}$$

where q is the charge of the particle, V is the RF cavity voltage, ψ is the accelerating phase, and $U(E)$ is the energy loss due to synchrotron radiation, which depends on the particle's energy.

In most practical applications, the changes in particle velocity and energy during acceleration are slower compared to the rate of phase change. Therefore, we treat them as constants for now. Under the assumption that the deviation of non-equilibrium particles from the equilibrium particle is small, the phase motion equation of the particle in the RF field is:

$$\ddot{\varphi} + 2\alpha_z \dot{\varphi} + \Omega^2 \varphi = 0 \tag{3}$$

where the damping factor is $\alpha_z = -\frac{1}{2T_0} \frac{dU}{dE}\big|_{E_0}$. The synchrotron oscillation frequency is given by[19]:

$$\Omega = \sqrt{\omega_{\text{rev}}^2 \frac{h\eta_c e\hat{V}_0 \cos\psi_s}{2\pi\beta c p_0}} \tag{4}$$

where T_0 is the revolution period, ω_{rev} is the revolution frequency, h is the harmonic number, and ψ_s is the synchronous phase. In a circular accelerator, particles periodically pass through a locally synchronized accelerating field in their orbit, oscillating around the synchronous phase with an oscillation frequency Ω. Multiple RF cavities are often used to provide the necessary accelerating field, and the RF voltage $V_0 \cos\psi_s$ is the total accelerating voltage seen by the particles during one complete revolution of the accelerator ring. The RF frequency is an integer multiple of the revolution frequency.

This means that the frequency design of the RF system must be strictly synchronized with the motion of the particles in the accelerator ring to ensure that particles can efficiently gain energy each time they pass through the RF cavity. By precisely controlling the voltage and phase in the RF cavity, the acceleration efficiency can be maximized, and the phase stability of the particle bunches can be regulated.

By solving the phase motion equation of the particle, we obtain:

$$\varphi = \hat{\varphi} e^{-\alpha_z t} \cos(\Omega t + \psi) \tag{5}$$

Similarly, by solving the energy motion equation, we derive the expression for energy oscillation:

$$\delta = \frac{\hat{\varphi}\Omega}{h\omega_0\eta_c} e^{-\alpha_z t} \sin(\Omega t + \psi) \tag{6}$$

where δ is the energy offset of the particle. A typical particle trajectory in longitudinal phase space is shown in Fig. 1. Both the particle's phase and energy undergo exponentially damped harmonic oscillations.

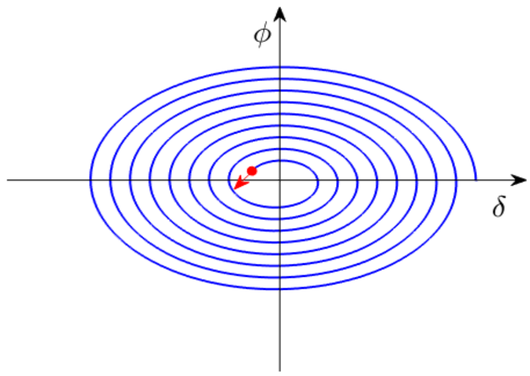

Fig. 1. The longitudinal phase space evolution of a single particle

III. SIMULATION DEVELOPMENT AND SINGLE-BUNCH TRACKING

From the above analysis, it can be concluded that during the injection process in the storage ring, individual particles undergo exponentially damped harmonic oscillations in phase space, and this is similar to the particle bunch. However, within the particle bunch, the initial phase and energy of each particle are different, making the analysis of the overall motion in phase space highly complex. In general, the particle bunch in phase space can be approximated as a two-dimensional Gaussian distribution, as shown in Fig. 2. This approximation simplifies the study of the bunch's overall motion.

Theoretically, for a Gaussian-distributed bunch, if we can measure the phase oscillation curve and bunch length oscillation curve after injection, we can deduce its initial two-dimensional Gaussian distribution at injection, including initial phase, initial bunch length, initial energy offset, initial energy spread, and initial energy chirp. These parameters are crucial for optimizing the injection system.

Based on the above theoretical foundation, to gain deeper insights into the longitudinal phase space evolution of the

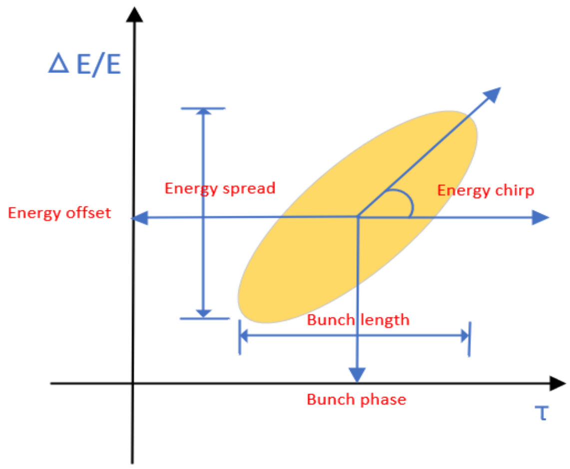

Fig. 2. Longitudinal phase space distribution and key parameters of the bunch

bunch during the injection process in the electron storage ring, we developed a single-bunch simulation tool using the mbtrack2 and PyQt5 software packages[20–22]. This tool is designed to track the longitudinal phase space distribution of the bunch after injection.

The user interface of the software is shown in Fig. 3. The interface is divided into the following sections:

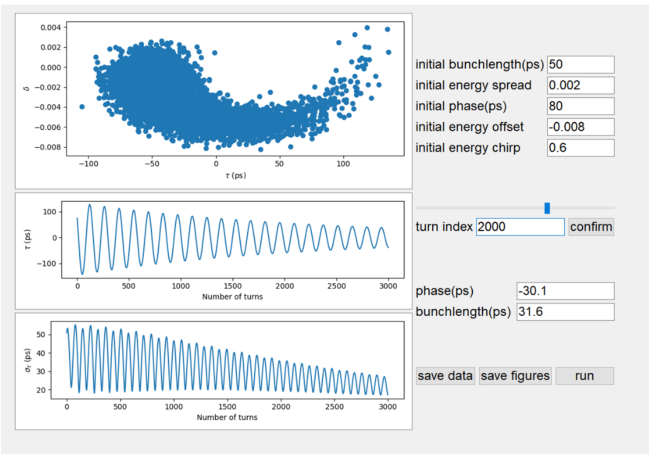

Fig. 3. Single beam longitudinal phase space simulation software interface

1. Left Section (Visualization Area): Top-left: Displays the longitudinal phase space distribution of the injected bunch for a specified number of turns (set on the right panel). Middle-left: Shows the phase evolution results from the beginning to the end of the simulation. Bottom-left: Displays the bunch length evolution results.

2. Right Section: Top-right (Initial Parameter Input Area): Includes the initial bunch length, initial energy spread, initial phase, initial energy offset, and initial energy chirp, used to control the initial phase space distribution of the injected bunch. Bottom-right (Operation Area): Allows the user to control the number of turns to view and displays the specific values of phase and bunch length for the current turn.

3. Bottom Section: Contains buttons for saving data, saving images, and starting the simulation.

The software supports reading external machine parameter files. By modifying these parameter files, it is theoretically possible to adapt the software to simulate any accelerator.

All simulations below use a single-bunch model, with $10,000$ particles simulated for $3,000$ turns (adjustable parameters). The simulation principles are as follows:

In mbtrack2, a particle is described as a point $(x, x', y, y', \tau, \delta)$ in six-dimensional phase space. x and y represent the horizontal and vertical positions, respectively. $x' = \frac{dx}{ds}$ and $y' = \frac{dy}{ds}$ represent the transverse momentum in the horizontal and vertical directions. τ is the time difference relative to the reference particle. $\delta = \frac{E-E_0}{E_0}$ represents the energy offset relative to the reference energy E_0.

If $\tau > 0$, the particle is delayed relative to the reference particle. In this case, we only track the longitudinal motion of τ and δ. Due to the effects of the RF cavity and synchrotron radiation damping, the iteration for τ and δ follows the code below:

$$\begin{cases} \tau_{n+1} = \tau_n + \eta T_0 \delta_n \\ \delta_{n+1} = \delta_n - \frac{U_0}{E_0} + \frac{V_0}{E_0} \cos\left(h\omega_{rev}\tau + \varphi_s\right) \\ \delta_{n+1} = \left(1 - \frac{2T_0}{\tau_\delta}\right)\delta_n + 2\sigma_\delta\sqrt{\frac{T_0}{\tau_\delta}} \times \epsilon \end{cases} \quad (7)$$

in this context, T_0 is a time constant; τ_δ is a time parameter related to δ; σ_δ is the standard deviation of δ; ϵ is a normally distributed random number to simulate the random processes of synchrotron radiation. This formula describes the energy dissipation and noise effects on particle motion due to synchrotron radiation.

Firstly, we tracked the longitudinal phase space evolution of the bunch. Fig. 4 shows the longitudinal phase space evolution under certain initial conditions. Each subfigure corresponds to a specific turn, with the X-axis representing the phase time offset τ and the Y-axis representing the energy offset δ. At the early stage of evolution, the phase space distribution of the bunch gradually bends, and noticeable filamentation appears at the tail of the bunch, indicating the influence of nonlinear effects. In the intermediate stage, the bunch's shape bends and stretches further, forming more complex structures, possibly due to the combined effects of synchrotron oscillations and radiation damping. In the later stage, the bunch gradually stabilizes into a more compact clump-like distribution, suggesting the system reaches equilibrium, with nonlinear effects weakening and internal energy exchange approaching balance. Overall, the process from initial perturbations to eventual stabilization reflects both the nonlinear effects and the self-stabilizing capacity of the system in an electron storage ring.

Additionally, simulations were performed for injected bunches with typical variations in initial distributions. The initial phase space parameters of these simulations are listed

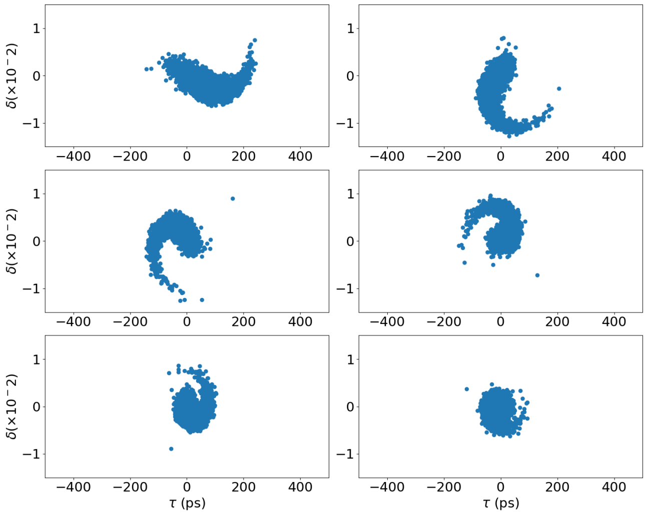

Fig. 4. Longitudinal phase space evolution of a single bunch

in Table. 1, and the initial phase space distribution and the reconstructed bunch length-phase two-dimensional distribution are shown in Fig. 5. In the two-dimensional distribution, the X-axis represents time, the Y-axis represents the charge density of the bunch, and the color ranges from blue to yellow, indicating density from low to high. It also reflects the center position of the bunch and the size of the bunch length, which is similar to the results obtained from the streak camera measurements.

Regarding energy chirp, it represents the variation of particle energy within the bunch over time. When the energy chirp is 0, the particles at the head and tail of the bunch have the same energy, meaning the bunch exhibits a regular elliptical distribution in phase space. When the energy chirp is non-zero, there is a discrepancy in energy between the head and tail of the bunch, resulting in a distribution in phase space that appears tilted at a certain angle. We define this tilt angle with a maximum value of 1 and a minimum value of -1 to represent the energy chirp.

Table 1. Simulated initial parameters for bunch injection.

Fig	Phase (ps)	Bunch length(ps)	Energy offset	Energy spread	Energy chirp(-1,1)
a	0	50	0.008	0.002	0
b	0	50	0	0.002	0
c	80	50	0	0.002	0
d	80	50	-0.008	0.002	0.6

In Fig. 5.a, the initial phase of the bunch is 0, the energy offset is 0.008, and the bunch length exhibits a maximum at the center of the phase oscillation, with minima at both ends. This phenomenon is the exact opposite of that shown in Fig. 5.c, where the bunch length exhibits a minimum at the center of the longitudinal oscillation, with maxima at both ends.

In Fig. 5.b, both the initial phase and energy offset are 0, with no longitudinal oscillation of the phase, achieving perfect injection.

In Fig. 5.d, the initial phase, energy offset, and energy chirp are all non-zero, which is more representative of practical injection scenarios. Near the extrema of the phase oscillation, a "winged" shape appears in the image, indicating a maximum in the bunch length.

Through these simulation results, it can be observed that the evolution differences after injection are quite obvious for bunches with different initial distributions. By adjusting these initial parameters, this simulation tool can model the phase space evolution of various injected bunches that may occur.

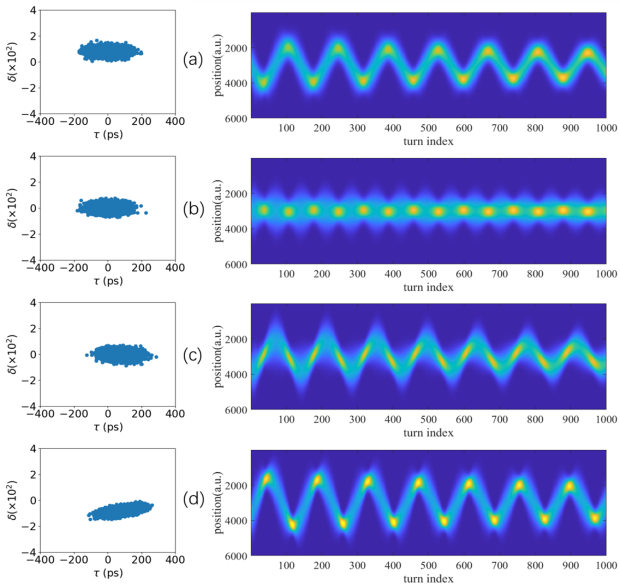

Fig. 5. injected bunch initial phase space distribution and bunch length-phase two-dimensional distribution evolution under different initial conditions.

IV. STORAGE RING BUNCH-BY-BUNCH PHASE AND LENGTH MEASUREMENT SYSTEM

The development of the simulation tool enables us to correlate the initial parameters of the injected bunch with its phase space evolution post-injection. By analyzing the bunch length and phase evolution data obtained from experiments, we can determine the initial parameters of the injected bunch. At present, the primary method for measuring phase and bunch length in the storage ring is the streak camera. However, since the streak camera cannot simultaneously provide high time resolution and a large dynamic range, we are limited to obtaining phase and bunch length data for the first few tens of turns post-injection, which is insufficient for follow-up analysis.

To address this, we developed a diagnostic system for individual bunches, which can compute the beam's three-dimensional position, charge, bunch length, and other parameters using raw data acquired from BPMs[23, 24]. Each data acquisition length covers several thousand turns. The phase

measurement accuracy for each bunch is 0.2 ps, and the bunch length measurement accuracy is 1 ps. The entire system includes both the data acquisition component and the offline processing component. The block diagram of the system is shown in Fig. 6.

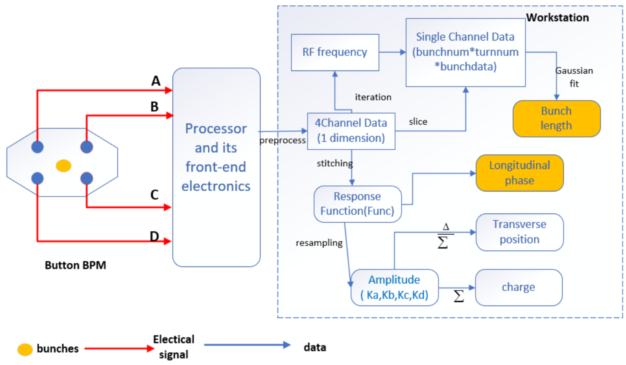

Fig. 6. Bunch-by-bunch bunch length and phase measurement system block diagram.

The data acquisition part uses a high-speed oscilloscope (6 GHz bandwidth, 16 GHz sampling rate, 16 bits) to collect button electrode coupling signals. Each acquisition can last several milliseconds, covering several thousand particle revolution periods. For the Shanghai Synchrotron Radiation Source, the RF frequency is 499.5 MHz, and the signal length for each bunch is approximately 2 ns. A single bunch signal can be sampled with 32 points, which well reconstructs the real signal waveform. The collected data is then processed by offline scripts for calculation.

In the offline processing script, the phase extraction algorithm is illustrated in Fig. 7. Considering the influences of bunch length and charge, a response function is constructed for each individual bunch (the red signal in Fig. 7.a represents the BPM signal of a single turn of a particular bunch, and the blue signal represents the constructed response function). Based on the response function, a lookup table is established, which traverses all phase values with a step size of 0.1 ps. The correlation function method is then used to identify the element in the lookup table that has the highest correlation with the measured data[25, 26].At this point, the zero-crossing point of the bunch signal is considered the phase of the bunch for that turn.

The calculation process for bunch length is illustrated in Fig. 8. Firstly, due to the difference between the system sampling rate and the storage ring RF frequency, it is necessary to accurately determine the single bunch signal length T based on the measured BPM signal. Then, the original BPM signal (a one-dimensional array) is sliced and restructured into a three-dimensional array (bunch signal slice * total turns * harmonic number) according to the signal length T. Fig. 8.a shows the signal waveform of a particular bunch in a particular turn from the original BPM signal. Next, harmonic analysis is performed on the sliced signal waveform to obtain the signal spectrum (Fig. 8.b), which is then multiplied by the system transfer impedance (Fig. 8.c) to yield the signal spectrum with a Gaussian distribution to be fitted. The system transfer impedance is calibrated using a streak camera, and the calibration coefficient is fixed for the same acquisition system. Finally, Gaussian fitting is applied to the calibrated signal spectrum, and the reciprocal of the frequency domain distribution σ in the fitting result represents the time domain bunch length for that bunch in that turn[27]. Table. 2 lists the machine parameters of SSRF.

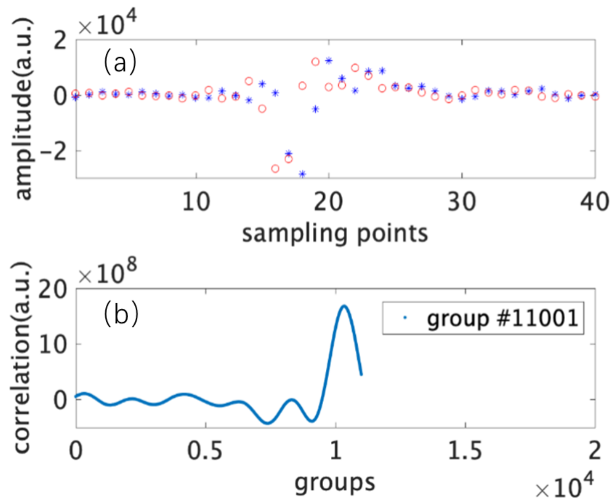

Fig. 7. a. Beam signal and response function. b. The calculation of the correlation coefficient.

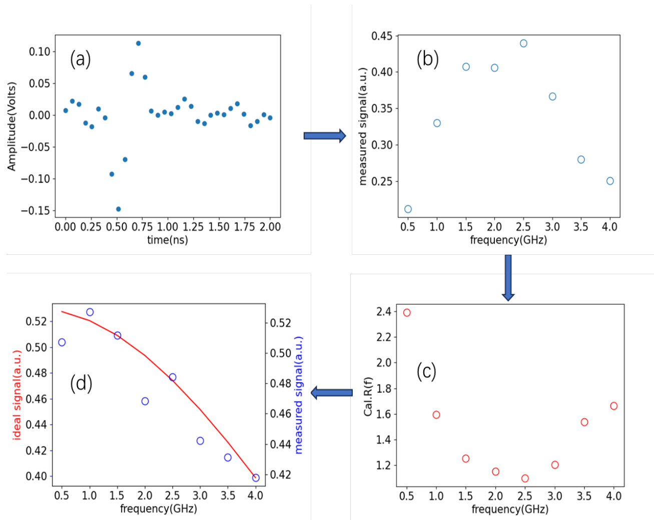

Fig. 8. a. Original BPM signal after sliced. b. Frequency domain distribution after FFT. c. System transmission impedance. d. Perform Gaussian fitting on the calibrated frequency domain signal.

Table 2. SSRF main parameters

Parameter	Value
Energy(E)	3.5GeV
Current(I_0)	200mA
RF frequency(f_{rf})	499.654MHz
Harmonic number(h)	720
Natural energy spread	0.001
Designed bunch length (σ)	18ps
Revolution Frequency(f_0)	694kHz
Synchrotron tune(υ_s)	0.007

V. BEAM EXPERIMENT

We collected multiple sets of data under the vacuum injection scenario in the Shanghai Synchrotron's storage ring. When there is a beam injection, the oscilloscope captures the trigger signal and records the data. Data is collected at regular intervals. Through the calculation of the developed bunch-by-bunch diagnostic system script, we obtained the longitudinal phase and bunch length evolution of a single bunch over several thousand turns during the injection process. A typical calculation result is shown in Fig. 9.

Fig. 9.a shows the evolution of the phase during the injection process. The entire evolution process follows a nearly exponential decay of sinusoidal oscillation, which matches the theory very well. The maximum amplitude does not exceed 100 ps, and of course, this is related to the beam energy introduced in the injector, the injection timing, and the initial phase-space distribution of the injected bunch. After 7 to 8 milliseconds of injection, the oscillation amplitude decays to within 20 ps.

Fig. 9.b shows the evolution of the bunch length during the injection process. The upper envelope of the bunch length also follows a trend of exponential decay. The initial oscillation amplitude reaches 80 ps. After 3000 turns, the bunch length oscillates and stabilizes around 20 ps. However, there is significant low-frequency noise in the bunch length calculation results. This is because the phase is the mean arrival time of the particles in the bunch, while the bunch length is the root-mean-square (RMS) value of the arrival time. Thus, compared to phase, the bunch length result is more susceptible to noise. In the future, we will further optimize the bunch length calculation algorithm.

To gain a more intuitive understanding of the beam's trajectory within the vacuum chamber, we reconstructed the two-dimensional distribution of bunch length and phase. First, low-pass filtering is applied to the phase and bunch length results to reduce noise. Then, under the assumption of a Gaussian distribution, the longitudinal distribution of the bunch for each turn is calculated and stored in a matrix. Finally, the 'imagesc' function is used to visualize the reconstructed 2D distribution.

Fig. 9.c shows the reconstructed result. This figure is similar to the measurement results of a streak camera, but it covers several thousand turns, extending beyond the dynamic range of the streak camera, and provides higher temporal resolution.

By zooming in and comparing different experimental samples, the details of the evolution can be observed. As shown in Fig. 10.a, at the maxima of the phase oscillation, the bunch length also reaches its maximum. When the phase is close to the center position, the bunch length is minimized. Fig. 10.b, on the other hand, shows the opposite pattern.

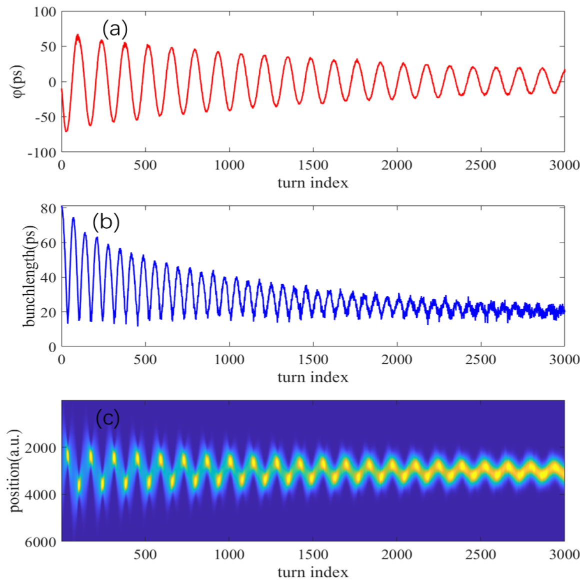

Fig. 9. a. Input bunch phase evolution. b. Injection bunch length evolution. c. Reconstructed bunch length-phase 2D distribution.

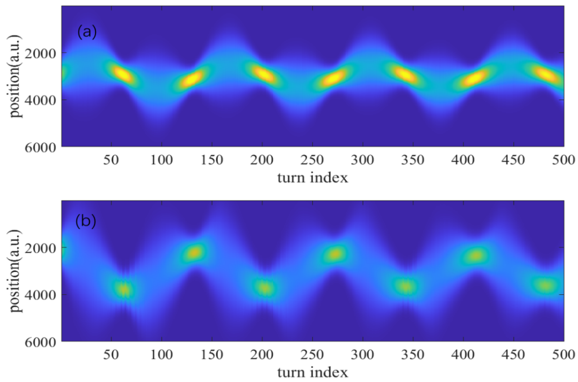

Fig. 10. Amplified 2D distribution of different experimental samples.

As mentioned earlier, by combining simulation results with experimental data, the initial parameters of the injected bunch in the experiment can be obtained. The specific implementation uses a genetic algorithm, where the variance between the simulation results and the experimental data is set as the fitness function to automatically optimize the simulation parameters. When the code runs to the preset number of iterations or the adaptive function reaches the desired accuracy, the final simulation results are derived. The simulation parameters are specified as follows: initial phase step of 0.5 ps, initial bunch length step of 1 ps, initial energy offset step of 0.01%, initial energy spread step of 0.01%, and initial energy

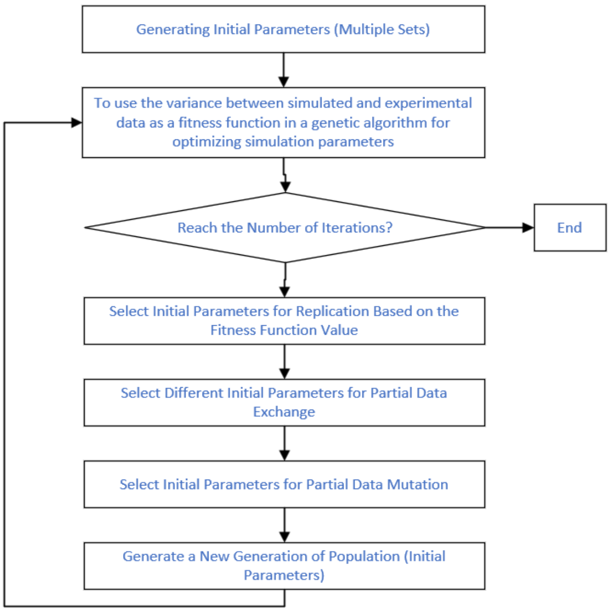

Fig. 11. Optimized initial parameter extraction genetic algorithm block diagram.

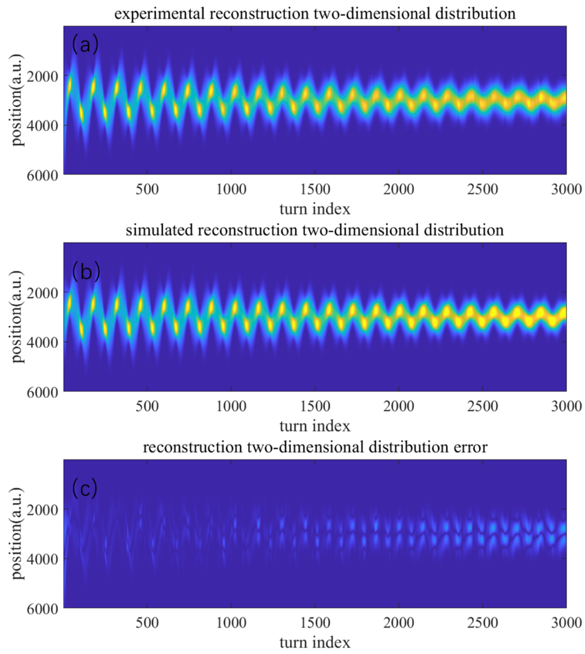

Fig. 12. Experimental and simulated bunch length-phase reconstructed 2D distribution and residual plot(2023.07.04).

chirp step of 0.01. The Pearson correlation coefficient for the phase of the optimal simulation data reaches approximately 0.99, with a variance of 5–10 (ps^2). The Pearson correlation coefficient for the bunch length reaches approximately 0.98, with a variance of 10–20 (ps^2). The detailed implementation block diagram is shown in Fig. 11.

We present a set of typical experimental and corresponding simulated reconstructed two-dimensional distribution images, with the dataset originating from the year 2023. As can be observed from Fig. 12, the simulation results exhibit a high degree of consistency with the experimental results, thereby validating the accuracy of the simulation software. This also reflects the high precision of the measurements obtained from the bunch-by-bunch diagnostic system, as well as the capability of this technique to accurately determine the initial parameters of the injected bunches in the experiment.

At the same time, we calculated the error's 2D distribution by subtracting the phase-bunch length 2D distribution of the experimental and simulation data. As shown in Fig. 12.c, the error between the experimental and simulation data gradually increases during the evolution over 3000 turns. This could be due to inconsistent longitudinal oscillation normalization frequencies or imperfect matching of the machine parameters. However, overall, the error remains within a relatively small range, especially within the first 1000 turns, where the experimental and simulation data match very well.

Additionally, Table. 3 lists the initial parameter calculation results for injection data over the years. It can be observed that, in the early stages, the initial bunch length does not start oscillating from the maximum value, indicating the presence of an initial energy chirp in the injected bunch. Afterward, the energy chirp approaches zero, and the initial bunch length tends to stabilize. Over time, the initial phase amplitude of the injected bunch also becomes smaller, the energy offset decreases, and the longitudinal position becomes more stable. In general, during this period, the SSRF injection system has been continuously optimized.

Table 3. Experimental initial parameters for bunch injection.

Experimental data	Phase (ps)	Bunch length(ps)	Energy offset	Energy spread	Energy chirp(-1,1)
20210906	-62.4	84.5	-0.0051	0.001	0
20210929	-9.7	81.4	-0.0045	0.0008	0
20211111	-11.3	31.1	-0.0032	0.0036	0.75
20211202	-48	80	-0.003	0.0012	0
20211224	21.1	24.3	-0.0028	0.0036	0.65
20220128	-11.3	45.1	0.0044	0.0045	0.86
20220218	-38.4	58.9	-0.0056	0.002	-0.4
20220318	-91.6	36.5	0.003	0.0062	0.8
20230508	25.5	50	-0.0045	0.001	0
20230613	35.6	50	-0.0065	0.001	0
20230704	55	50	-0.002	0.0012	0
20230831	-20	50	-0.0018	0.001	0
20231017	-34	46	0	0.0015	0
20231107	-30	60	0	0.0021	0
20231205	-10	60	-0.001	0.0033	0
20240103	20	60	0	0.0023	0

VI. SUMMARY AND CONCLUSIONS

Through the bunch-by-bunch data processing script, the evolution of the initial phase and bunch length of the injected bunch over several thousand turns can be obtained. However,

the initial energy offset, energy spread, and energy chirp of the injected bunch cannot be determined.

Subsequently, we developed simulation software for the single-bunch injection phase space evolution based on the mbtrack2 and PyQt5 software packages. By providing the initial parameters of the injected bunch, the software can simulate phase space evolution data under various injection conditions. Then, through a genetic algorithm, we optimized the initial parameters by aligning the simulation data with experimental data, thus obtaining the initial parameters of the experimental data. The acquisition of these parameters provides a powerful tool for the optimization of the injection system.

Additionally, using the simulation software, a large amount of single-bunch injection phase space evolution data can be generated, and the initial phase space distribution of these bunches is known. Machine learning can then be used to train a large number of simulation samples to analyze experimental data and determine the initial injection parameters. In the future development of the simulation software, instead of simulating the phase space distribution, the original signal distribution of the bunch after injection will be directly simulated. This will serve as the training sample, allowing for the direct analysis of the raw sampling signals without going through the bunch-by-bunch diagnostic system, making it easier and faster to obtain the initial injection parameters.

ACKNOWLEDGEMENTS

We would like to express our sincere gratitude to Dr. Zhou Yimei from the Shanghai Synchrotron Radiation Facility for her assistance in data acquisition during the experiment. We are also deeply thankful to Professor Leng Yongbin for his patient guidance and encouragement throughout the experiment.

[1] N. S. Sereno, F. R. Lenkszus. Feedback correction of injection errors using digital signal-processing techniques. Phys.Rev.Spec.Top-Ac, 2007, 10(1): 012803. doi: 10.1103/PhysRevSTAB.10.012803

[2] M. Aiba, M. Boge, A. Saa Hernandez, *et al.*, Longitudinal top-up injection for small aperture storage rings, in *Proceedings of IPAC2014*, (Dresden, Germany), pp.1842-1844. doi:10.18429/JACoW-IPAC2014-WEOAA0

[3] B. Jiang, Z. Zhao, S. Tian, *et al.*, Using a double frequency rf system to facilitate on-axis beam accumulation in a storage ring, Nucl. Instrum. Methods A **814** (2016) 1–5. doi:10.1016/j.nima.2016.01.024

[4] M. Aiba, Review of top-up injection schemes for electron storage rings, in *Proceedings of IPAC2018*, (Vancouver, BC, Canada), pp.1745–1750. doi:10.18429/JACoW-IPAC2018-WEXGBE1

[5] S. Jiang, G. Xu, On-axis injection scheme based on a triple-frequency rf system for diffraction-limited storage rings, Phys.Rev.Accel.Beams **21** 110701(2018). doi:10.1103/PhysRevAccelBeams.21.110701

[6] P. Kuske, J. Li, M. Aiba, Longitudinal acceptance measurement at an electron storage ring, Phys.Rev.Accel.Beams **23** 030701(2020). doi: 10.1103/PhysRevAccelBeams.23.030701

[7] L. MedinaMedrano, R. Calaga, H. Timko, *et al.*, Studies of longitudinal beam losses at lhc injection, in *Proceedings of IPAC2021*,(Campinas, SP, Brazil),pp.4164-4167. doi: 10.18429/JACoW-IPAC2021-THPAB199

[8] G. H. Wang, B. C. Jiang, J. H. Tan, *et al.*, Study on crab-cavity-based longitudinal injection scheme and prototype realization of c-band crab cavity for electron storage rings, Nucl. Sci. Tech. **34** (7) (2023) 102.doi: 10.1007/s41365-023-01257-5

[9] L. L. Tang, P. Lu, B. G. Sun, Z. Zeran, *et al.*, Bunch-by-bunch phase measurement and longitudinal instabilities diagnostics at hefei light source, High Power Laser and Particle Beams, 2021, 33: 104001, doi: 10.11884/HPLPB202133.210164

[10] D. Teytelman, J. Fox, W. Cheng, *et al.*, Control and measurements of longitudinal coupled-bunch in stabilities in the ATF damping ring, in *Proceedings of PAC2007*, (Albuquerque, New Mexico, USA) pp. 584–586. doi: 10.1109/PAC.2007.4440286

[11] J. Byrd, W. H. Cheng, S. DeSantis, *et al.*, Nonlinear longitudinal dynamics studies at the als, in *Proceedings of PAC1999* (Cat. No. 99CH36366), Vol. 1, IEEE, 1999, pp. 382–386.

[12] J. Byrd, S. De Santis, Longitudinal injection transients in an electron stor age ring, Phys.Rev.Spec.Top-Ac **4** 024401(2001). doi: 10.1103/PhysRevSTAB.4.024401

[13] S. Moniri, P. Taherparvar, The multiturn transverse injection scheme us ing short pulse nonlinear kicker into the 3.5 gev synchrotron storage ring, Pramana– J. Phys. **98** 6(2024) doi: 10.1007/s12043-023-02692-0

[14] M. Kim, I. Hwang, S. J. Park, *et al.*, Tracking study of transient behaviors at beam injection of the pls-ii ring, Journal of the Korean Physical Society **63** (2013), pp.2072–2079.doi: 10.3938/jkps.63.2072

[15] J. Corbett, A. Fisher, X. Huang, *et al.*, Injected beam dynamics in spear3, in: Conf. Proc. C100523:TUPEC039, 2010, no. SLAC-PUB-15103, Citeseer, 2012.

[16] T. Watanabe, T. Fujita, M. Masaki, *et al.*, Measurement of longitudinal dynamics of injected beam in a storage ring, in *Proceedings of IPAC2011*, (San Sebastián, Spain), pp.2978-2980.

[17] Z. B. Sun, L. Shang, F. L. Shang, *et al*, Simulation study of longitudinal injection scheme for HALS with a higher harmonic cavity system, Nucl.Sci.Tech. **113** 30(2019). doi: 10.1007/s41365-019-0627-x

[18] N. Sudar, Y. Ding, An analytical backtracking method for electron beam longitudinal phase space shaping, arXiv preprint arXiv:2208.03973(2022). doi: 10.48550/arXiv.2208.03973

[19] P. Baudrenghien, Low-level rf-part i: Longitudinal dynamics and beam based loops in synchrotrons, arXiv preprint arXiv:1201.2597 (2012).

[20] K. Bane, P. Emma, Litrack: a fast longitudinal phase space tracking code with graphical user interface, in*Proceedings of PAC2005*,(Knoxville, Tennessee), pp. 4266–4268.

[21] N. Yamamoto, A. Gamelin, R. Nagaoka, *et al.*, Investigation of longitudi nal beam dynamics with harmonic cavities by using the code mbtrack, in*Proceedings of PAC2019*, (Melbourne, Australia), pp. 178–180. doi: 10.18429/JACoW-IPAC2019-MOPGW039

[22] A. Gamelin, W. Foosang, R. Nagaoka, *et al*., mbtrack2, a collective effect library in python, in*Proceedings of PAC2021*, (Campinas, SP, Brazil), pp.282–285. doi: 10.18429/JACoW-IPAC2021-MOPAB070

[23] Y. M. Deng, Y. B. Leng, X. Y. Xu, *et al*., Ultrahigh spatiotemporal resolution beam signal reconstruction with bunch phase compensation, Nucl.Sci.Tech. **35** 89(2024). doi: 10.1007/s41365-024-01444-y

[24] X. Yang, H. S. Wang, Y.M. Zhou, *et al*., Determining beam transverse absolute position by triangulation of multi-electrode signal phase differences, Nucl.Sci.Tech. **35** 133(2024). doi: 10.1007/s41365-024-01498-y

[25] Y. M. Zhou, H. J. Chen, S. S. Cao, *et al*., Bunch-by-bunch longitudinal phase monitor at ssrf, Nucl.Sci.Tech. **29** 113(2018). doi: 10.1007/s41365-018-0445-6

[26] Y. Zhou, Z. Chen, B. Gao, *et al*., Bunch-by-bunch phase study of the transient state during injection, Nucl. Instrum. Methods A **78** 2018,pp.68-80. doi: 10.1016/j.nima.2019.163273

[27] H. S. Wang, X. Yang, Y. B. Leng, *et al*., Bunch-length measurement at a bunch-by-bunch rate based on ttime-requency-domain joint analysis techniques and its application, Nucl.Sci.Tech. **35** 80(2024). doi: 10.1007/s41365-024-01443-z